ELSEVIER

Cardiovascular Pathology 10 (2001) 59–68

CARDIOVASCULAR PATHOLOGY

Diagnosis of human coronary atherosclerosis by morphology-based Raman spectroscopy

Hendrik P. Buschman[a,b,*], Jason T. Motz[b], Geurt Deinum[b], Tjeerd J. Römer[a], Maryann Fitzmaurice[c], John R. Kramer[d], Arnoud van der Laarse[a], Albert V. Bruschke[a], Michael S. Feld[b]

[a]*Leiden University Medical Center, Leiden, Netherlands*
[b]*Massachusetts Institute of Technology, Cambridge, MA, USA*
[c]*University Hospitals of Cleveland and Case Western Reserve University, Cleveland, OH, USA*
[d]*The Cleveland Clinic Foundation, Cleveland, OH, USA*

Received 17 May 2000; received in revised form 28 February 2001; accepted 12 March 2001

Abstract

Background: Recent studies have shown that chemical composition and morphology, rather than anatomy (degree of stenosis), determine atherosclerotic plaque instability and predict disease progression. Current clinical diagnostic techniques provide accurate assessment of plaque anatomy, but have limited capability to assess plaque morphology in vivo. Here we describe a technique for a morphology-based diagnosis of atherosclerosis in the coronary arteries using Raman spectroscopy that can potentially be performed in vivo using optical fiber technology. **Methods:** Raman tissue spectra were collected from normal and atherosclerotic coronary artery samples in different stages of disease progression ($n = 165$) from explanted transplant recipient hearts ($n = 16$). Raman spectra from the elastic laminae (EL), collagen fibers (CF), smooth muscle cells (SMC), adventitial adipocytes (AA) or fat cells, foam cells (FC), necrotic core (NC), cholesterol crystals (CC), β-carotene containing crystals (β-C), and calcium mineralizations (CM) were used as basis spectra in a linear least squares-minimization (LSM) model to calculate the contribution of these morphologic structures to the coronary artery tissue spectra. **Results:** We developed a diagnostic algorithm that used the fit-contributions of the various morphologic structures to classify 97 coronary artery samples in an initial calibration data set as either nonatherosclerotic, calcified plaque, or noncalcified atheromatous plaque. The algorithm was subsequently tested prospectively in a second validation data set, and correctly classified 64 (94%) of 68 coronary artery samples. **Conclusions:** Raman spectroscopy provides information about the morphologic composition of intact human coronary artery without the need for excision and microscopic examination. In the future, it may be possible to use this technique to analyze the morphologic composition of atherosclerotic coronary artery lesions and assess plaque instability and disease progression in vivo.

Keywords: Atherosclerosis; Coronary artery disease; Raman spectroscopy; Morphology; Diagnosis

1. Introduction

The use of Raman spectroscopy has great potential for diagnostic imaging of human coronary artery disease in vivo [1–3]. Recent studies have shown that chemical composition and morphology, rather than anatomy (degree of stenosis), determine atherosclerotic plaque instability and predict disease progression and the risk of life-threatening complications such as thrombosis and acute plaque hemorrhage [4–16]. Current diagnostic imaging techniques such as intravascular ultrasound (IVUS), MRI, and angiography provide predominantly anatomic information about the extent of luminal stenosis, but yield only limited information about lesion composition [17–23]. A number of studies have shown that quantitative chemical information regarding lesion composition can be acquired from Raman spectra of normal and atherosclerotic arterial tissue using mathematical modeling [24–30]. We now report that quantitative

* Corresponding author. Present address: Twente Institute for Neuromodulation, Medisch Spectrum Twente, P.O. Box 50000, 7500 KA Enschede, The Netherlands. Tel.: +31-53-4872840, +31-53-4872802; fax: +31-53-4873100.

E-mail address: r.buschman@rrd.nl (H.P. Buschman).

1054-8807/01/$ – see front matter
PII: S1054-8807(01)00063-1

morphologic information regarding lesion composition can also be acquired from coronary arteries by Raman spectroscopy using a modification of the mathematical model. Secondly, we show that this morphologic information can be used for diagnostic purposes. To our opinion, the chemical and morphologic information obtained by Raman spectroscopy can be the basis of more powerful diagnostic assessment of human coronary artery disease in the future.

One of the early studies of Raman spectroscopy in atherosclerosis used a principal component analysis (PCA) model of the Raman spectra [26]. In this technique, the principal components (or basis spectra) contributing to the variance in the Raman tissue spectra, were extracted mathematically. Calculated model fit-coefficients for the principal components were then used as the basis of a diagnostic algorithm to classify coronary artery tissues as either nonatherosclerotic or calcified plaque or noncalcified plaque. In this mathematical model, the principal components (or basis spectra) do not necessarily have specific chemical or morphologic counterparts. Therefore, although it can be used to diagnose arterial tissue as atherosclerotic or nonatherosclerotic, it does not provide specific chemical or morphologic information about the lesion.

One of the great advantages of Raman spectroscopy over other diagnostic techniques is its ability to identify the biochemical components of tissue and to determine their tissue concentrations in situ. Recent studies using a second linear least squares-minimization (LSM) model take advantage of the biochemical information in Raman spectra, using Raman spectra of biochemical constituents extracted from arterial tissue as a basis set in a LSM model to obtain the calculated model fit-coefficients (or relative weight fractions) of the biochemical constituents in the tissue [27,28]. The relative weight fractions of total cholesterol and calcium salts were then used in an algorithm to classify the arterial tissues as normal or atherosclerotic as in the PCA model [29]. More importantly, this model provides a quantitative analysis of the chemical composition of the arterial tissue that may contribute to the diagnosis of the plaque's instability.

In principal, both quantitative chemical and morphologic information regarding atherosclerotic lesion composition can be obtained from the same Raman spectrum. The objective of the present study was to analyze coronary artery tissue by modeling of Raman tissue spectra using the spectra of morphologic structures rather than biochemical components as a basis set. Basis spectra for the model were obtained from morphologic structures commonly observed in the normal artery wall and in atherosclerotic plaque, including collagen fibers (CF), the internal and external elastic laminae (EL), smooth muscle cells (SMC), adventitial adipocytes (AA) or fat cells, foam cells (FC), necrotic core (NC), cholesterol crystals (CC), β-carotene containing crystals (β-C), and calcium mineralizations (CM) [30]. These basis spectra were then used to linearly fit the spectra of an initial calibration set of coronary artery specimens. Using the fit-contributions of the various morphologic structures, an algorithm was developed to classify the arteries as atherosclerotic or nonatherosclerotic as in the biochemical model. To test the diagnostic performance of this morphology-based model, the algorithm was subsequently applied to a second, prospective, validation set of coronary arteries.

2. Materials and methods

2.1. Tissue preparation

Human coronary artery samples ($n = 200$) from 16 patients, exhibiting different stages of atherosclerosis, were obtained from explanted recipient hearts within 1 hour after heart transplantation. Seven patients had heart failure due to dilated cardiomyopathy and nine due to severe ischemic heart disease. Immediately after dissection from the explanted heart, the artery segments were rinsed with neutral-buffered saline solution, snap-frozen in liquid nitrogen, and stored at $-85°C$ until use. The artery samples were collected in two sets, the first containing 113 (calibration set) and the second, 87 samples (prospective validation set).

These artery samples were used for macroscopic and microscopic Raman spectroscopy studies. For the macroscopic study, the samples (97 and 68, from the first and second sets, respectively) were warmed passively to room temperature, cut open longitudinally, placed in an aluminum holder with the lumen side upwards, and examined under $\times 10$ magnification for selection of the region to be evaluated [27]. After spectroscopic examination, each spot interrogated was marked with a small spot of colloidal ink, and fixed in 10% neutral-buffered formalin.

Details of the collection of the Raman spectra using a microspectrometer were described previously [30]. In short, unstained, transverse tissue sections (6–8 μm) were cut from the coronary artery samples. Four sections of each sample were mounted on glass microscope slides and stained for light microscopic examination, whereas serial unstained transverse sections were mounted on BaF_2 or MgF_2 flats (International Scientific Products, Tarrytown, NY and Spectra-Tech, Stamford, CT), kept moist with phosphate buffered saline (pH 7.4), and transferred to the microscope stage for spectroscopic experiments. No coverslip was used. Under white light illumination, the major morphologic structures were selected and recorded on videotape under $\times 10$ and $\times 63$ magnification.

2.2. Histology

The formalin-fixed macroscopic tissue samples were routinely processed, paraffin-embedded, and cut through the marked locations in 5-μm thick sections, stained with

hematoxylin and eosin, and examined by two experienced cardiovascular pathologists who were blinded to the outcome of the Raman spectroscopy analysis. The tissue sections were classified according to the updated Systemized Nomenclature of Human and Veterinary Medicine (SNoMed) [31] and have been used previously [26–29]. The samples in both the calibration and validation data sets were diagnosed as either (1) normal ($n = 12$ and 1), (2) intimal fibroplasia ($n = 61$ and 25), (3) atherosclerotic plaque ($n = 3$ and 0), (4) atheromatous plaque ($n = 6$ and 16), (5) calcified atherosclerotic plaque ($n = 1$ and 3), (6) calcified atheromatous plaque ($n = 7$ and 13), (7) calcified fibrosclerotic plaque ($n = 5$ and 10), or (8) calcified intimal fibroplasia ($n = 2$ and 0, respectively). Because some of these categories had small sample numbers, the eight categories were condensed into three diagnostic classes for the development of the diagnostic algorithm: Class I, nonatherosclerotic tissue (Categories 1 and 2; $n = 73$ and 26); Class II, noncalcified atherosclerotic plaque (Categories 3 and 4; $n = 9$ and 16); and Class III, calcified atherosclerotic plaque (Categories 5–8; $n = 15$ and 26).

2.3. Instrumentation and Raman spectroscopy

The macroscopic and microscopic Raman spectra were obtained using the Raman spectroscopy system shown in Fig. 1. Detailed descriptions of the instrumentation for macroscopic and microscopic measurements and the data processing can be found elsewhere [30]. In short, near-infrared (NIR) laser light (830 nm) was generated by an Ar^+-pumped Ti:sapphire laser system (Coherent Innova 90/Spectra Physics 3900S, Coherent, Santa Clara, CA). The laser output was band pass-filtered (Kaiser Optical Systems HLBF, Ann Arbor, MI) and, by insertion of a

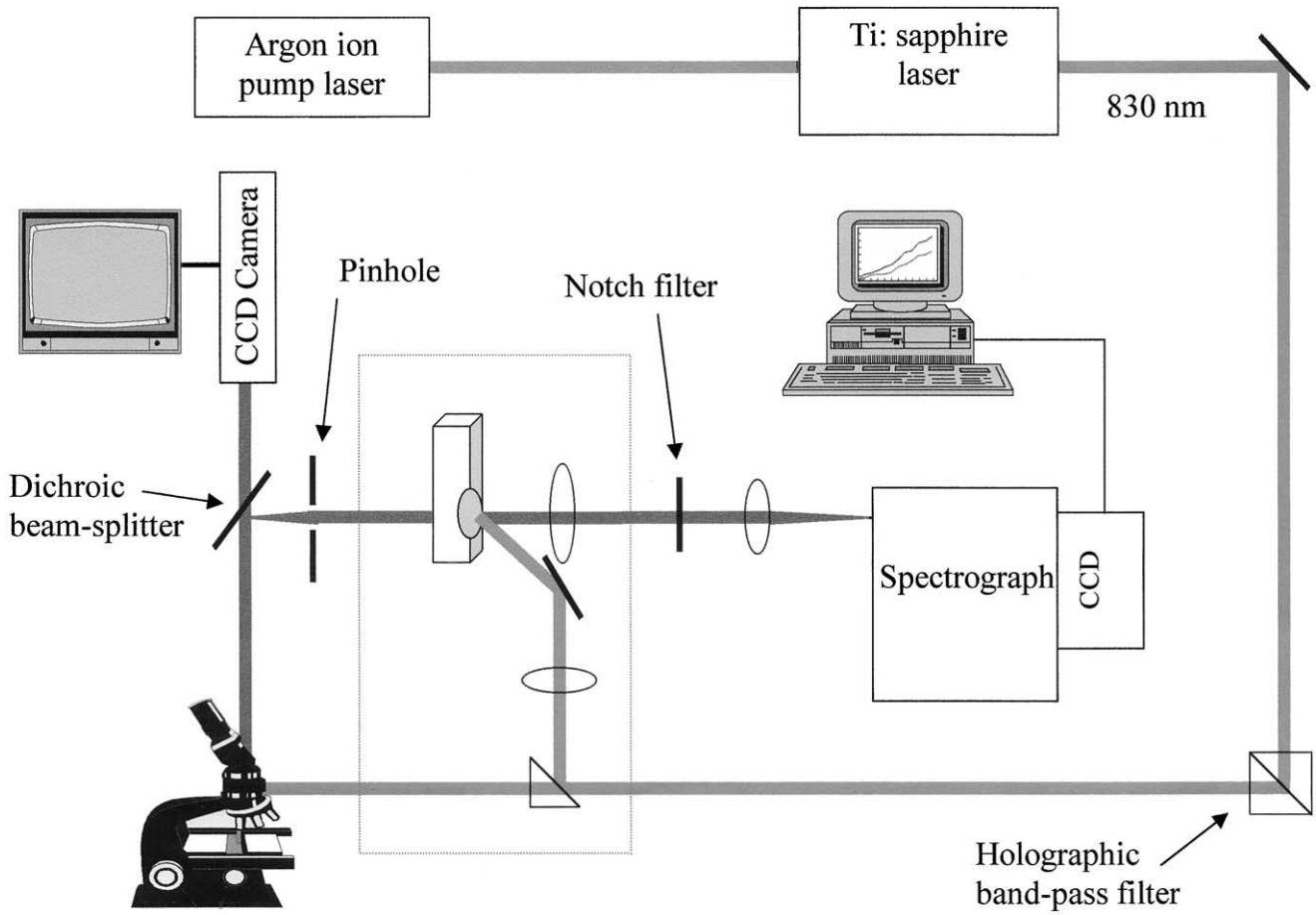

Fig. 1. Schematic representation of the combined Raman macrospectroscopy and confocal microspectroscopy system. NIR laser light (830 nm) is delivered by an Ar^+-pumped Ti:sapphire laser system and passes through a holographic laser band pass filter. Using a prism, the light is directed either to the microscope system or the macroscopic system. When directed to the microscope system, the light is focused onto a tissue sample through a high numerical aperture microscope objective. The scattered light is collected by the same objective, passes the beam splitter, and is focussed onto a pinhole (P), which enables confocal resolution. The remaining light is passed through a Notch filter to remove Rayleigh-scattered laser light, and is then coupled into the spectrometer using a lens. The dichroic beam splitter is used to direct either collected Raman scattered light from the sample to the spectrometer–CCD system, or white light images to the video camera system. When directed to the macroscopic system, the light is projected onto a coronary artery sample, and the Raman scattered light is collected by a lens, Notch-filtered, and projected into the spectrometer–CCD system. Raman signals are read from the CCD, collected by a personal computer and stored on hard disk for later analysis.

prism, either projected onto the tissue sample in the macroscopic setup, or projected into a confocal microscope and focused onto the tissue section with a $\times 63$ infinitely corrected water immersion objective (Zeiss Achroplan, NA 0.9). In the macroscopic setup, Raman-scattered light from the tissue (sampling volume 1–2 mm^3) was collected with a lens, Notch-filtered, and focused onto the entrance slit of a Chromex 250IS/SM spectrophotometer (Chromex, Albuquerque, NM). In the microscope setup (sampling volume approximately 1 μm^3), the Raman light scattered from the tissue was collected with the same objective that was used to focus light onto the sample, passed through a pinhole (giving the system its confocal characteristic), Notch-filtered, and projected onto the entrance slit of the spectrophotometer. Inside the spectrograph, a grating dispersed light onto a deep-depletion CCD detector (Princeton Instruments, Princeton, NJ) cooled to $-110°C$. The CCD interface (ST130, Princeton Instruments), along with data storage and processing, was rendered on a personal computer.

For the macroscopic measurements, the laser power was 350 mW, and the signal collection time was 10–100 s. For the microscopic measurements, the laser power was 80–120 mW, and the signal collection time was 60–360 s. The Raman spectra were collected in the range between 400 and 2000 cm^{-1} (resolution 8 cm^{-1}).

Each spectrum was frequency-calibrated and corrected for chromatic variations in spectrometer system detection. A fourth-order polynomial was fit to each spectrum and subtracted from the spectrum to correct for remaining tissue fluorescence [27]. The macroscopic tissue spectra were modeled in the 680–1800 cm^{-1} Raman shift range as a linear combination of the morphologic structure basis spectra by LSM. This Raman shift range was chosen, because this range contains most spectral information.

2.4. Morphologic spectral analysis

In this study, the Raman spectra of morphologic structures commonly observed in atherosclerotic plaque were used as basis spectra. The Raman basis spectra were obtained by microspectroscopy from the following 10 morphologic structures: CF, the internal and external EL, SMC, AA or fat cells, FC, NC, CC, β-C, and CM (Fig. 2). In a previous study, we have shown that the spectral variation for any one morphologic structure is very small, indicating that the chemical composition of any morphologic structure is relatively constant [30]. Therefore, in this study, each morphologic structure was represented by a single Raman spectrum. Furthermore, we have previously shown that the chemical composition of FC and NC are nearly identical as determined by this Raman spectroscopic technique. Therefore, in the present study, we represent these two morphologic structures by a single Raman spectrum (FC/NC). Similarly, we have shown previously that the spectra of the internal and external EL are nearly identical, and we have represented them by a single spectrum as well (EL).

The morphologic structure Raman spectra were normalized with respect to their maximum peak intensity. All spectra in the two data sets could be modeled accurately with the final set of eight morphologic basis spectra. The Raman spectral model calculated the fractional fit-contribution of seven of the morphologic structures. The eighth structure, β-carotene, is an intense Raman scatterer that

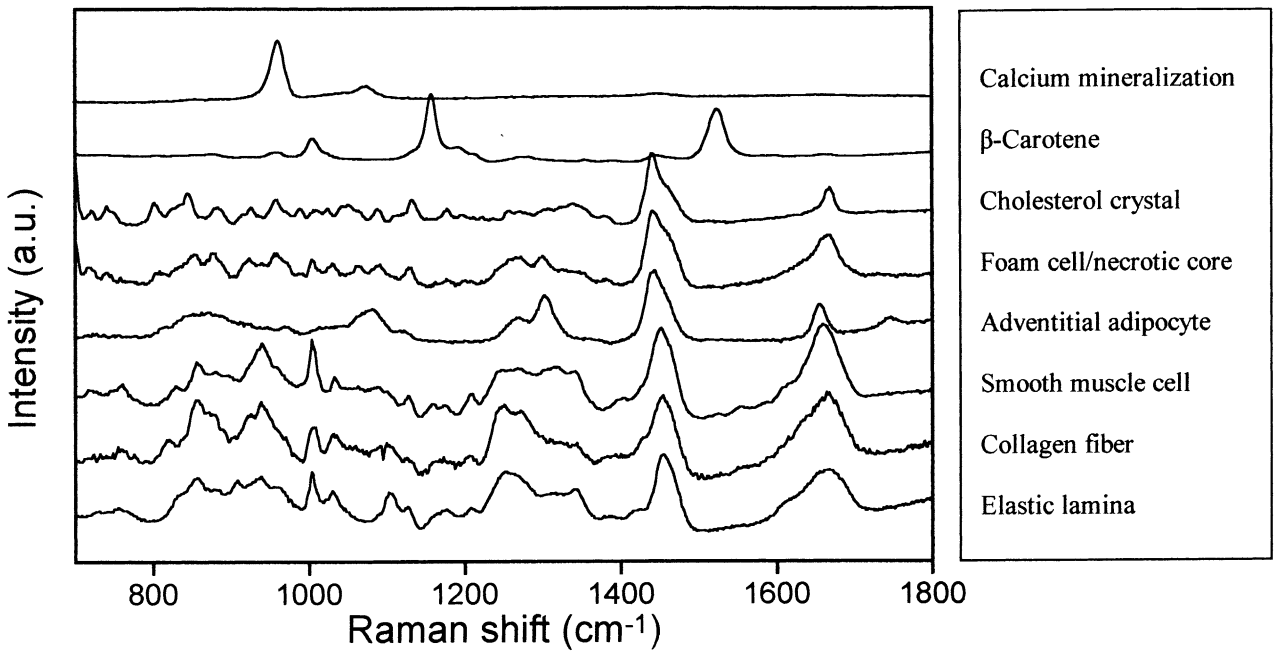

Fig. 2. Raman spectra of the eight selected coronary artery morphologic structures.

often contributes to coronary artery Raman spectra, but is present only in low concentrations. For this reason, its spectrum was included in the spectral model, but no fractional fit-contribution was calculated.

In calcified atherosclerotic plaques, CM often occupy large volumes of the tissue examined by Raman spectroscopy. To obtain information about the remaining noncalcified regions, and to compare the morphologic structure fractional fit-contributions among the different disease classes, we renormalized the spectra of calcified plaques, neglecting the contribution of calcium mineralization, and calculated the morphologic structure fractional fit-contributions of the noncalcified regions (denoted by X_{NCR}), as was done previously in calculating the relative weight fractions in the biochemical model [27–29].

2.5. Algorithm development

The relative fit-contribution of each morphologic structure to the spectra in the calibration data set was used to develop an algorithm to classify the tissue into one of the three diagnostic classes. The method of logistic regression was used to generate a discriminant score, R_i, based on a linear combination of relative fit-contributions (C_l) of each morphologic structure l as $R_i = \alpha_i + \beta_{1i}C_1 + \beta_{2i}C_2 + \ldots$ with α_i being a constant and β_{li} an adjustable coefficient for each morphologic structure. This method was chosen over discriminant analysis, because logistic regression does not make any assumptions about the normalcy of the fit-coefficients [31].

Using maximum likelihood estimation with the software package STATA (Release 5.0, Stata, College Station, TX), we determined the probability that an artery sample j is nonatherosclerotic (P_{jI}), or contains a noncalcified atherosclerotic plaque (P_{jII}), or contains a calcified atherosclerotic plaque (P_{jIII}) as

$$P_{jI} = \frac{1}{1 + e^{Rj1} + e^{Rj2}},$$

$$P_{jII} = \frac{e^{Rjt}}{1 + e^{Rj1} + e^{Rj2}}, \text{ and } P_{jIII} = 1 - P_{jII} - P_{jI},$$

which sum to one [31]. Furthermore, using a likelihood-ratio test on the initial calibration data set, it was determined which morphologic structure relative fit-contributions were significant for diagnosis, and what diagnostic thresholds for these relative fit-contributions correctly classify the most samples. The algorithm so developed was then used to prospectively classify the artery samples in the second validation data set.

To determine the level of error in the model, it is necessary to analyze the signal/noise ratio (SNR) of the spectra being used. Because the microscopic Raman artery spectra of the morphological model could be collected for arbitrarily long times, they are virtually noise-free (see Fig. 2). Therefore, the limiting source of error in the model is due to noise in the macroscopic spectra of the intact arteries. The in vitro system is shot noise-limited, and therefore, the noise for any given

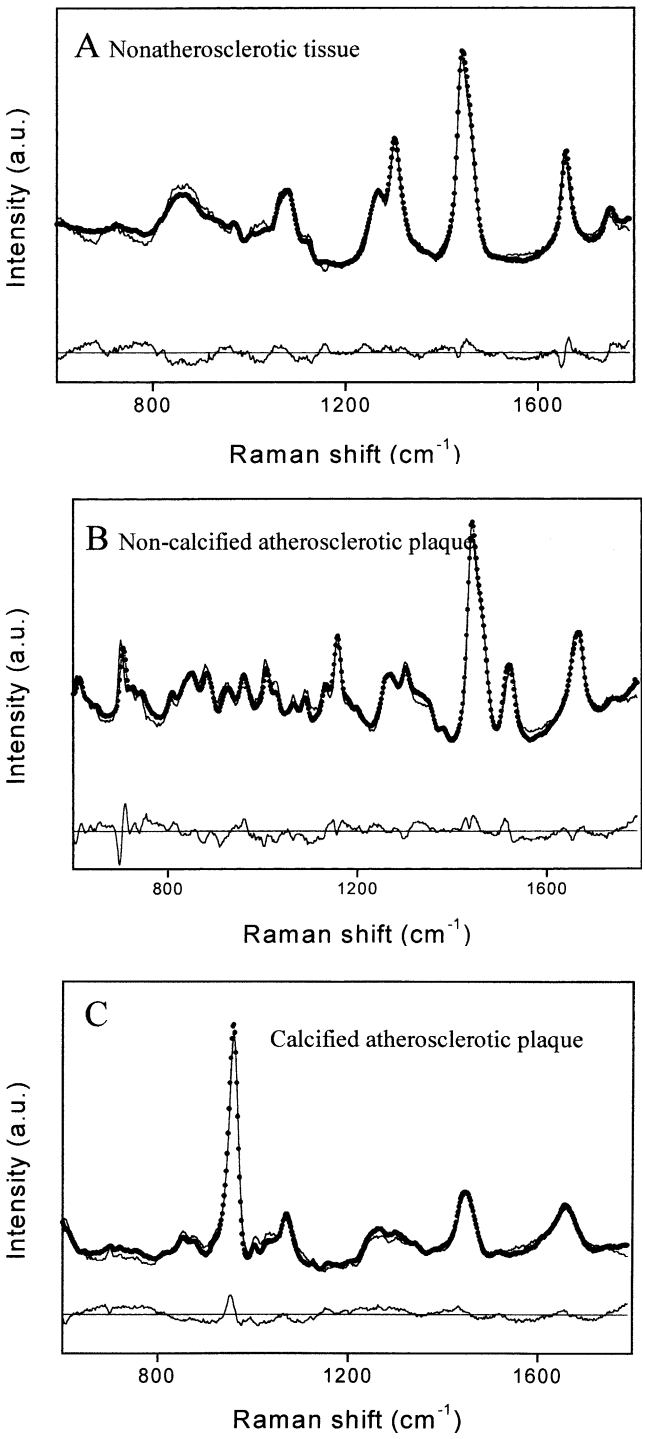

Fig. 3. Examples of fitting the morphologic Raman spectral model to macroscopic spectra: (A) a nonatherosclerotic tissue, (B) a noncalcified atherosclerotic plaque, and (C) a calcified atherosclerotic plaque. The solid line is the macroscopic spectrum, and the dotted line the model fit. The lower line in each graph is the residual between macroscopic spectrum and model fit.

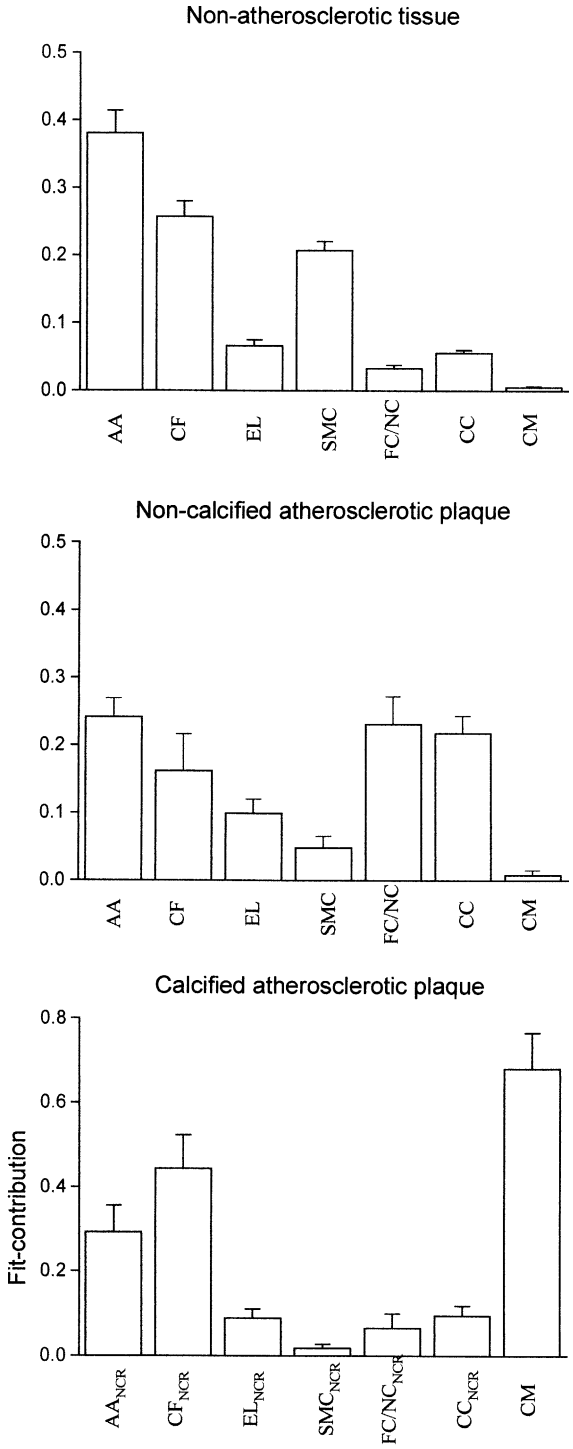

Fig. 4. The results of the fit contribution of seven morphologic structures to the calibration data set, and the diagnostic algorithm classification as: (A) nonatherosclerotic tissue, (B) noncalcified atherosclerotic plaque, or (C) calcified atherosclerotic plaque. AA: adventitial adipocytes, CF: collagen fibers, EL: internal/external elastic lamina, SMC: smooth muscle cells, FC/NC: foam cells/necrotic core, CC: cholesterol crystal, CM: calcium mineralizations. X_{NCR}: the relative contribution of X in the noncalcified region. Data shown are mean ± S.E.M. Note: different scaling in C.

sample is equal to the square root of the signal. Following standard multivariate analysis techniques [31], the concentration error is proportional to the noise in the spectrum

$$E = \boldsymbol{N} \times \boldsymbol{B},$$

where $\boldsymbol{B} = P^{\mathrm{T}}(PP^{\mathrm{T}})^{-1}$, is the calibration vector for the morphologic basis spectrum of interest, and $\boldsymbol{N}$ is the noise in the sample [32].

3. Results

3.1. Morphologic spectral modeling of macroscopic coronary artery spectra

Fig. 3 shows macroscopic Raman spectra collected from coronary artery samples representing each of the three diagnostic classes (normal coronary artery, noncalcified atherosclerotic plaque, and calcified atherosclerotic plaque), together with LSM model fits. Residuals (data minus the fit) are shown on the same scale. For all spectra, the calculated fit agrees well with the measured spectrum, which suggests that the morphologic basis spectra are a reasonably complete representation of the Raman spectra of the macroscopic tissue samples.

The Raman spectra of all 97 coronary artery samples in the calibration data set, which were classified by a pathologist into one of the three diagnostic classes, were analyzed in the same way. The mean ± S.D. of the relative fit-contribution of all eight selected morphologic structures in nonatherosclerotic tissue (I), noncalcified atherosclerotic plaque (II), and calcified atherosclerotic plaque (III) are shown in Fig. 4. This figure clearly shows that Raman spectroscopic modeling is able to detect morphologic changes in coronary artery tissue. The morphologic Raman model showed, as expected, that nonatheroscler-

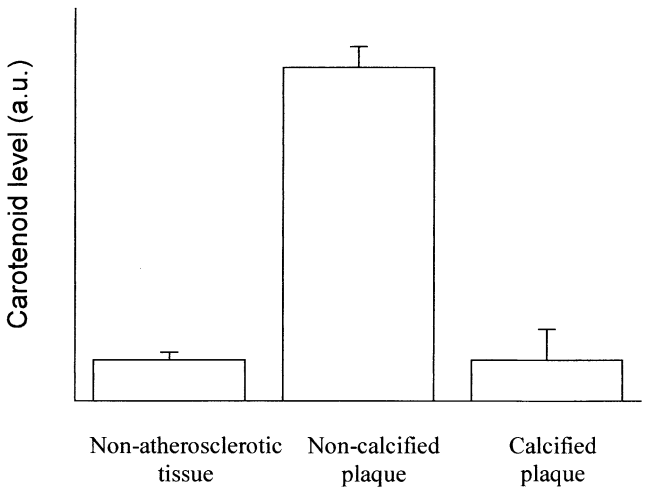

Fig. 5. The spectral contribution of β-carotene in the calibration data set in relation to the three diagnostic categories. The carotenoid level is expressed in arbitrary units.

otic tissue consisted mainly of AA, CF, EL, and SMC (Fig 4A). In nonatherosclerotic artery, the intima is thin and therefore, the contribution of the adventitial layer (which contains a relatively large amount of adipose tissue) to the spectroscopically examined tissue volume is large, because the NIR laser light penetrates through the entire vessel wall. In noncalcified and calcified atherosclerotic plaque, the morphologic Raman model revealed a dramatic change of the morphologic composition with progression of disease. In noncalcified atherosclerotic plaques, where the intima is thickened, the AA contribution decreased, whereas the contribution of FC/NC and CC increased (Fig 4B) due to accumulation of lipids in the plaque. Raman spectra of calcified atherosclerotic plaques were dominated by the CM contribution (Fig 4C). The contribution of AA_{NCR} and CF_{NCR} in calcified atherosclerotic plaque was smaller than that of AA and CF in noncalcified atherosclerotic plaque.

Although the concentration of β-carotene in arterial tissue is low, the modeling outcome showed large differences in the contribution of carotenoids among the disease classes (Fig 5). The largest contribution was found in noncalcified atherosclerotic plaques, since β-carotene is a lipophilic substance that dissolves easily in the NC.

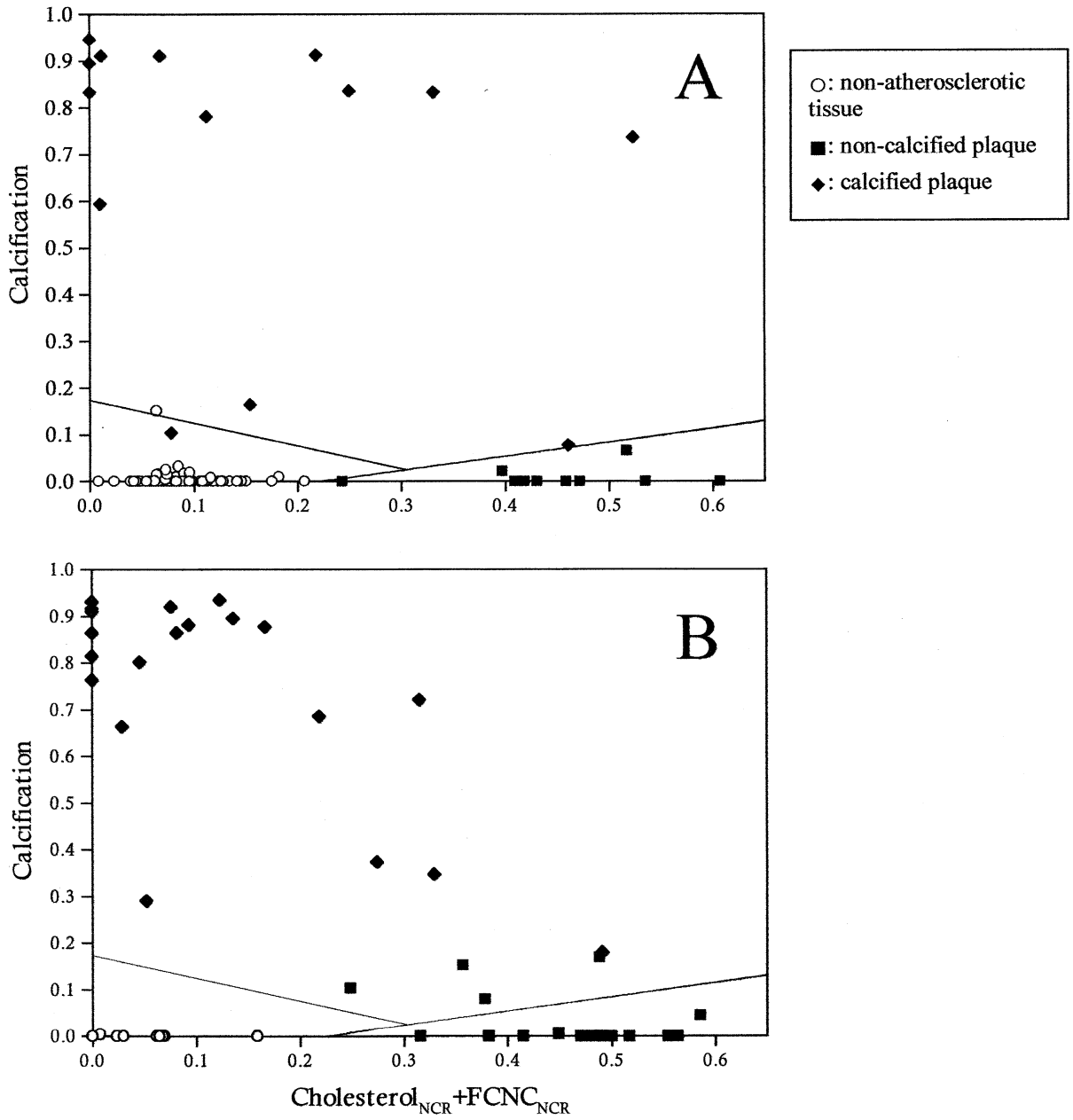

Fig. 6. The diagnostic algorithm based on fit contributions of CM and CC_{NCR} + FC/NC_{NCR}. (A) Shows the algorithm developed with the initial calibration data set. (B) Shows the results of the prospective validation data set. The symbols refer to the diagnostic classes: nonatherosclerotic tissue (○), noncalcified atherosclerotic plaque (■), and calcified atherosclerotic plaque (◆).

3.2. Diagnostic algorithms

Using logistic regression, we determined that an optimal separation of the data into three diagnostic classes was obtained using the fit-contributions of CM and $FC/NC_{NCR}+CC_{NCR}$, with $P<.0001$ using a likelihood-ratio test. In addition, the likelihood-ratio test determined that no improvement in classification resulted from inclusion of any of the remaining morphologic structures ($P<.05$). The discriminant scores were determined to be $R_{j1}=-420.4+1870.0\times(FC/NC_{NCR}+CC_{NCR})-6094.3\times CM$, and $R_{j2}=-8.3+23.3\times(FC/NC_{NCR}+CC_{NCR})+47.6\times CM$.

The fit-contributions of CM and $FC/NC_{NCR}+CC_{NCR}$ of each artery sample can be plotted in a decision diagram (Fig 6A), using the corresponding R_1 and R_2 values. The border separating the regions of nonatherosclerotic tissue and noncalcified atherosclerotic plaque is given by PI = PII, which is a line described by the equation $CM=-0.07+0.31\times(FC/NC_{NCR}+CC_{NCR})$. The border separating the regions of nonatherosclerotic tissue and calcified atherosclerotic plaque is given by PI = PIII, and has the equation $CM=0.17-0.48\times(FC/NC_{NCR}+CC_{NCR})$. The line separating the regions of noncalcified atherosclerotic plaque and calcified atherosclerotic plaque is given by PII = PIII, and has the equation $CM=-0.07+0.30\times(FC/NC_{NCR}+CC_{NCR})$. For 95 of the 97 (98%) samples in the initial calibration data set, the decision determined by the Raman-based diagnostic algorithm correlated with that of the pathologist.

Subsequently, this algorithm was used prospectively to classify the artery samples of the second validation data set into one of the three diagnostic classes (Fig 6B). Prospectively, the algorithm result agreed with that of the pathologist for 64 of 68 samples (94%). Comparison of the pathologic and Raman spectroscopic diagnoses for both data sets is shown in Table 1.

Table 1
Comparison of pathologic diagnosis with that of the morphology-based Raman diagnostic algorithm.

Raman diagnosis				
Pathology diagnosis	I	II	III	Total
Calibration data set				
I	72	0	1	73
II	0	9	0	9
III	1	0	14	15
Total	73	9	15	97
Prospective data set				
I	26	0	0	26
II	0	12	4	16
III	0	0	26	26
Total	26	12	30	68

The classes are (I) nonatherosclerotic tissue, (II) noncalcified plaque, and (III) calcified plaque.

Because the in vitro Raman system used for collecting macroscopic artery spectra is shot-noise limited, the NIR techniques used in acquiring the data have resulted in extremely high SNR spectra. The average peak-to-peak is less than 0.04 counts on normalized spectra. Calculation of error on the fit-coefficients of diagnostic morphologic components yield a three-S.D. error of 0.041 for CM, and a three-S.D. error of 0.036 for $FC/NC_{NCR}+CC_{NCR}$.

4. Discussion

Recent studies have shown that chemical composition and morphology, rather than anatomy (degree of stenosis), determine atherosclerotic plaque instability and predict disease progression and the risk of life-threatening complications such as thrombosis and acute plaque hemorrhage [4–12]. For example, the presence of cholesterol esters may soften the plaque, whereas crystalline-free cholesterol may have the opposite effect [13,14]. The presence of FC and other inflammatory cells may also play a role in plaque instability [15,16].

Current diagnostic-imaging techniques, including IVUS, MRI, and angiography provide an accurate assessment of plaque anatomy, but have limited capability to quantitatively assess plaque morphology or chemical composition in vivo. Coronary angiography, still the "gold standard" for diagnosing coronary artery disease, shows the degree of luminal stenosis, but provides no chemical or morphologic information about the plaque. In fact, unstable atherosclerotic plaques are often "silent" on angiography [19–22]. IVUS, the most accurate and quantitative technique currently in clinical use, uses the reflection of acoustical waves delivered by an intravascular catheter to probe tissue density and provide imaging information [17]. It has advanced our understanding of atherosclerosis significantly by demonstrating extensive atherosclerosis in coronary arteries that appear normal on angiography. However, although IVUS can identify the presence of an atheroma core, it cannot specifically identify FC or CC and does not provide any chemical information [22]. MRI has the advantage of being a noninvasive technique, and uses radio waves generated by applying a magnetic field gradient to again probe tissue density and provide imaging information. Like IVUS, it can be used to analyze anatomy and, to a lesser extent, morphology [23]. However, conventional proton MRI techniques used clinically largely ignore and often suppress the chemical shift information. Thus, currently, plaque morphology and chemical composition can only be assessed by microscopic examination of excised tissues after endarterectomy or atherectomy.

Previous studies have shown that a linear LSM Raman spectroscopy model can be used to quantitatively assess the chemical composition of coronary artery atherosclerotic plaque [24–29]. In the present study, we

have shown that a modification of that Raman spectroscopy model can also be used to identify the microscopic morphologic structures comprising the plaque, and that the pathological state of the artery could be accurately assessed using a diagnostic algorithm based on the relative contribution of these microscopic morphologic structures to the macroscopic arterial Raman spectrum. The diagnostic algorithm, constructed with an initial calibration data set, was tested in a second prospective data set, where it predicted disease classification with 94% accuracy.

CM and $FC/NC_{NCR}+CC_{NCR}$, which were found to increase with severity in atherosclerotic plaque, were the most predictive parameters for classifying arterial tissue as nonatherosclerotic, calcified plaque, or noncalcified plaque. β-C also had predictive value in discriminating the three diagnostic categories, and an algorithm could be made using β-C and CM as diagnostic parameters. Its diagnostic power, however, was less than that for CM and $FC/NC_{NCR}+CC_{NCR}$.

Initially, eight atherosclerotic classes were used for comparison with previous studies using the PCA and chemical models. These eight classes were reduced to three, because it was not possible to individually distinguish all eight diagnostic (SNoMed) classes using our current morphology-based Raman spectroscopic model. This is partly due to differences in the number of samples in each of the diagnostic classes, as described previously [29], but also due to the inability of the current Raman spectroscopic model to discriminate subtle morphologic differences between certain diagnostic classes. For example, using the current Raman spectroscopic model, it was not possible to distinguish atherosclerotic plaques (which contain FC only) from atheromatous plaques (which contain both FC and NC). This is due, in part, to the small numbers of atherosclerotic plaques in the study set. It is also due, in part, to the similarity of the FC and NC basis spectra [30]. This is most likely due to the fact that the NC is largely an extracellular accumulation of cytoplasmic lipid released from FC when they undergo necrosis or apoptosis.

Currently, the diagnosis of atherosclerosis and assessment of plaque stability and extent of disease progression is most accurately done by post procedural pathologic examination of excised tissue. The morphologic structures selected as basis spectra in the Raman model represent those structures that are commonly used in pathologic diagnosis and classification of atherosclerotic lesions by light microscopy. On pathologic examination, the presence of FC, NC, and CC are significant predictors of plaque instability and disease progression [4–16]. The present study showed that Raman spectroscopic analysis of these same morphologic structures could be used to diagnose atherosclerotic lesions in intact coronary arteries, without the need for microscopic examination. This suggests that, with further development, Raman spectroscopy can provide not only quantitative chemical information, but also quantitative morphologic information regarding atherosclerotic lesion composition, such as the presence of CC, not readily available in current diagnostic imaging techniques such as IVUS, MRI, and angiography.

The current chemical- and morphology-based Raman spectroscopy models also have potential limitations. The explicit nature of these models requires a thorough understanding of arterial tissue and its chemical or morphologic composition. Although extensively studied, the biochemistry and morphology of atherosclerosis are still imperfectly understood, and small but diagnostically significant differences in chemical composition or morphology may be missed with these types of modeling, as was seen for NC and FC in the morphologic model.

It should also be noted that while useful for comparison to previous studies, the eight-class SNoMed classification system does not distinguish between stable and unstable plaque, and some of the morphologic features associated with unstable plaque, such as inflammatory cells other than FC, were not included as basis spectra in the model. Therefore, further studies are needed to ascertain whether our current morphology-based Raman spectroscopic model can, in fact, provide the type of quantitative morphologic information necessary to distinguish stable from unstable atherosclerotic plaque.

5. Conclusions

Diagnostic classification of atherosclerotic plaques in human coronary arteries can be performed accurately by quantitative assessment of their morphologic composition using Raman spectroscopy. The rapid and nondestructive nature of Raman spectroscopy provides the opportunity to diagnose coronary artery plaques in vivo, when applied in a clinical setting using optical fiber technology. So used, this technique cannot only classify an atherosclerotic lesion, but may provide an in vivo quantitative assessment of its morphologic features, such as the presence of FC, NC, and CC, which may be used to assess plaque instability and the extent of disease progression, and thereby, the risk of life-threatening complications such as thrombosis and acute plaque hemorrhage. So used, this technique may provide insight into as yet poorly understood dynamics in the evolution of atherosclerotic lesions and the effects of lipid-lowering and other therapies.

Acknowledgments

Financial support from the Interuniversity Cardiology Institute of the Netherlands (ICIN D96.2158/MH), the Netherlands Heart Foundation (95.134), and the NIH (grant: P41RR02594) is gratefully acknowledged. The research was conducted at the MIT Laser Biomedical Research Center, Cambridge, MA, USA.

References

[1] Baraga JF, Feld MS, Rava RP. In situ optical histochemistry of human artery tissue using near infrared Fourier transform Raman spectroscopy. Proc Natl Acad Sci USA 1992;89:3473–7.

[2] Manoharan R, Baraga JJ, Feld MS, Rava RP. Quantitative histochemical analysis of human artery using Raman spectroscopy. J Photochem Photobiol B 1992;16:211–33.

[3] Manoharan R, Wang Y, Feld MS. Histochemical analysis of biological tissues using Raman spectroscopy. Spectrochim Acta Part A 1996;52:215–49.

[4] Steinberg D, Witztum JL. Lipoproteins and atherogenesis. Current concepts. JAMA, J Am Med Assoc 1990;264:3047–52.

[5] Loree HM, Tobias BJ, Gibson LJ, Kamm RD, Small DM, Lee RT. Mechanical properties of model atherosclerotic lesion lipid pools. Arterioscler Thromb 1994;14:230–4.

[6] Libby P. Molecular bases of the acute coronary syndromes. Circulation 1995;91:2844–50.

[7] Richardson PD, Davies MJ, Born GV. Influence of plaque configuration and stress distribution on fissuring of coronary atherosclerotic plaques. Lancet 1989;2:941–4.

[8] Fuster V, Badimon L, Badimon J, Chesebro J-T. The pathogenesis of coronary artery disease and the acute syndromes. N Engl J Med 1992;326:242–50, 310–8 (two articles).

[9] Woolf N, Davies MJ. Arterial plaque and thrombus formation. Sci Am Sci Med 1994;38–47.

[10] Fishbein MC, Siegal RJ. How big are coronary atherosclerotic plaques that rupture? Circulation 1996;94:2662–6.

[11] Mann JM, Davies MJ. Vulnerable plaque relation of characteristics to degree of stenosis in human coronary arteries. Circulation 1996;94: 928–31.

[12] Wexler L, Brundage B, Crouse J, Detrano R, Fuster V, Maddahi J, Rumberger J, Stanford W, White R, Taubert K. Coronary artery calcification: pathophysiology, epidemiology, imaging methods, and clinical implications: a statement for health professionals from the American Heart Association. Circulation 1996;94:1175–92.

[13] Libby P, Schoenbeck U, Mach F, Selwyn AP, Ganz P. Current concepts in cardiovascular pathology: the role of LDL cholesterol in plaque rupture and stabilization. Am J Med 1998;104:14S–8S.

[14] Kullo IJ, Edwards WD, Schwartz RS. Vulnerable plaque: pathobiology and clinical implications. Ann Intern Med 1998;129:1050–60.

[15] Matsuda Y, Kramer JR, Matsuda M. Progression and regression of coronary artery disease-linkage of clinical, pathologic, and angiographic findings. Clin Cardiol 1995;18:412–7.

[16] Burke AP, Farb A, Malcolm GT, Liang Y-H, Smialwk JE, Virmani R. Plaque rupture and sudden death related to exertion in men with coronary artery disease. JAMA, J Am Med Assoc 1999;281: 921–6.

[17] Peters RJG, Kok WE, Havenith MG, Rijsterborgh H, van der Wal AC, Visser CA. Histopathologic validation of intracoronary ultrasound imaging. J Am Soc Echocardiogr 1994;7:230–41.

[18] Feld S, Ganim M, Carell ES. Comparison of angioscopy, intravascular ultrasound imaging and quantitative coronary angiography in predicting clinical outcome after coronary intervention in high risk patients. J Am Coll Cardiol 1996;28:97–105.

[19] Tuczu EM, Berkalp B, DeFranco AC, Ellis SG, Goormastic M, Whitlow PL, Franco I, Raymond RE, Nissen SE. The dilemma of diagnosing coronary calcification: angiography versus intravascular ultrasound. J Am Coll Cardiol 1996;28:832–8.

[20] Glagov S, Zarins CK, Giddens DP, Ku DN. Hemodynamics and atherosclerosis: insights and perspectives gained from studies of human arteries. Arch Pathol Lab Med 1988;112:1018–31.

[21] Mintz GS, Popma JJ, Pichard AD, Kent KM, Satler LF, Chuang YC, Ditrano CJ, Leon MB. Patterns of calcification in coronary disease. A statistical analysis of intravascular ultrasound and coronary angiography. Circulation 1995;91:1959–65.

[22] Topol EJ, Nissen SE. Our preoccupation with coronary luminology the dissociation between clinical and angiographic findings in ischemic heart disease. Circulation 1995;92:2333–42.

[23] Toussaint JF, LaMuraglia GM, Southern JF, Fuster V, Kantor HL. Magnetic resonance images lipid, fibrous, calcified, hemorrhagic, and thrombotic components of human atherosclerosis in vivo. Circulation 1996;94:932–8.

[24] Brennan JFB, Wang Y, Dasari RR, Feld MS. Near-infrared Raman spectrometer systems for human tissue studies. Appl Spectrosc 1997;51: 201–8.

[25] Wolthuis R, Bakker-Schut TC, Caspers PJ, Buschman HPJ, Römer TJ, Bruining HA, Puppels GJ. Raman spectroscopic methods for in vitro and in vivo tissue characterisation. In: Mason WT, editor. Fluorescent and luminescent probes. 2nd ed. London: Academic Press, 1999. pp. 433–55.

[26] Deinum G, Rodriquez D, Römer TJ, Brennan JF, Fitzmaurice M, Myles JL, Kramer, Lees RS, Feld MS. Principal component analysis as a method to correlate the Raman spectrum and the pathology of human coronary artery tissue. Appl Spectrosc 1999;53:938–42.

[27] Brennan JF, Römer TJ, Lees RS, Tercyak AM, Kramer JR, Feld MS. Determination of human coronary artery composition by Raman spectroscopy. Circulation 1997;96:99–105.

[28] Salenius JP, Brennan JF, Miller A, Wang Y, Aretz T, Sacks B, Dasari RR, Feld MS. Biochemical composition of human peripheral arteries examined with near-infrared Raman spectroscopy. J Vasc Surg 1998;27:710–9.

[29] Römer TJ, Brennan JF, Fitzmaurice M, Feldstein ML, Deinum G, Myles JL, Kramer JR, Lees RS, Feld MS. Histopathology of human coronary atherosclerosis by quantifying its chemical composition with Raman spectroscopy. Circulation 1998;97:878–85.

[30] Buschman HP, Deinum G, Motz JT, Fitzmaurice M, Kramer JR, van der Laarse A, Bruschke AV, Feld MS. Raman microspectroscopy of human coronary atherosclerosis; biochemical assesment of cellular and extracellular morphologic structures in situ. Cardiovasc Pathol 2001;10:69–82.

[31] Cote RA. Updated version of the Systemized Nomenclature Of Human And Veterinary Medicine (SNoMed): a glossary for pathologic classification. Northfield, IL: The College of American Pathologists, 1993.

[32] Shama S. Applied multivariate techniques. New York: Wiley, 1996.